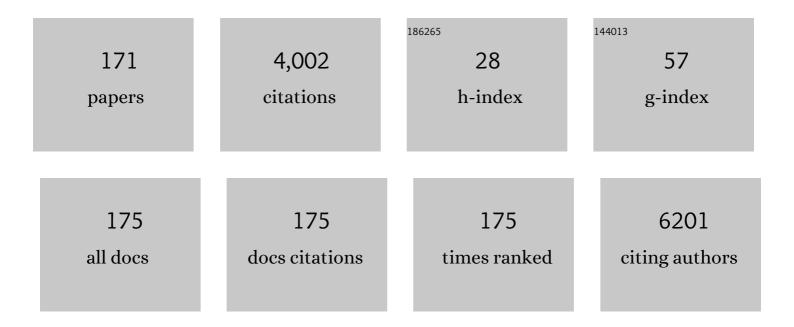
Saveria Santangelo

List of Publications by Year in descending order

Source: https://exaly.com/author-pdf/8010174/publications.pdf Version: 2024-02-01



#	Article	IF	CITATIONS
1	Light Emission Properties of Thermally Evaporated CH3NH3PbBr3 Perovskite from Nano- to Macro-Scale: Role of Free and Localized Excitons. Nanomaterials, 2022, 12, 211.	4.1	1
2	Evaluation of Entropyâ€Stabilized (Mg _{0.2} Co _{0.2} Ni _{0.2} Cu _{0.2} Zn _{0.2})O Oxides Produced via Solvothermal Method or Electrospinning as Anodes in Lithiumâ€Ion Batteries. Advanced Functional Materials, 2022, 32, .	14.9	31
3	High-Entropy Spinel Oxides Produced via Sol-Gel and Electrospinning and Their Evaluation as Anodes in Li-Ion Batteries. Applied Sciences (Switzerland), 2022, 12, 5965.	2.5	18
4	Comparative life cycle assessment of Fe2O3-based fibers as anode materials for sodium-ion batteries. Environment, Development and Sustainability, 2021, 23, 6786-6799.	5.0	12
5	Effect of Germanium Incorporation on the Electrochemical Performance of Electrospun Fe2O3 Nanofibers-Based Anodes in Sodium-Ion Batteries. Applied Sciences (Switzerland), 2021, 11, 1483.	2.5	5
6	On the plasmon-assisted detection of a 1585 cmâ^1 mode in the 532 nm Raman spectra of crystalline α -Fe2O3/polycrystalline NiO core/shell nanofibers. Applied Physics Letters, 2021, 118, .	3.3	4
7	Evaluation of Electrospun Self-Supporting Paper-Like Fibrous Membranes as Oil Sorbents. Membranes, 2021, 11, 515.	3.0	2
8	Photocatalytic degradation of methylene blue dye by porous zinc oxide nanofibers prepared via electrospinning: When defects become merits. Applied Surface Science, 2021, 557, 149830.	6.1	22
9	Photocatalytic Degradation of Methylene Blue Dye by Electrospun Binary and Ternary Zinc and Titanium Oxide Nanofibers. Applied Sciences (Switzerland), 2021, 11, 9720.	2.5	9
10	High-density polyethylene/carbon nanotubes composites: Investigation on the factors responsible for the fracture formation under tensile loading. Journal of Polymer Research, 2021, 28, 1.	2.4	0
11	Bacterial-cellulose-derived carbonaceous electrode materials for water desalination via capacitive method: The crucial role of defect sites. Desalination, 2020, 492, 114596.	8.2	18
12	Effect of Hematite Doping with Aliovalent Impurities on the Electrochemical Performance of α-Fe2O3@rGO-Based Anodes in Sodium-Ion Batteries. Nanomaterials, 2020, 10, 1588.	4.1	10
13	Comparing the Performance of Nb ₂ O ₅ Composites with Reduced Graphene Oxide and Amorphous Carbon in Li―and Naâ€ŀon Electrochemical Storage Devices. ChemElectroChem, 2020, 7, 1689-1698.	3.4	23
14	Structure, Defects, and Magnetism of Electrospun Hematite Nanofibers Silica-Coated by Atomic Layer Deposition. Langmuir, 2020, 36, 1305-1319.	3.5	18
15	Frontier Research Applications of Electro-spun Nanomaterials in Healthcare. Current Nanomaterials, 2019, 4, 4-5.	0.4	0
16	Exploiting the Condensation Reactions of Acetophenone to Engineer Carbonâ€Encapsulated Nb ₂ O ₅ Nanocrystals for Highâ€Performance Li and Na Energy Storage Systems. Advanced Energy Materials, 2019, 9, 1902813.	19.5	49
17	Electrospun Ag/PMA Nanofibrous Scaffold as a Drug Delivery System. Current Nanomaterials, 2019, 4, 32-38.	0.4	4
18	Light-matter Interaction Under Intense Field Conditions: Nonlinear Optical Properties of Metallic-dielectric Nanostructures. Current Nanomaterials, 2019, 4, 51-62.	0.4	2

#	Article	IF	CITATIONS
19	Compositional and Mineralogical Analysis of Marine Sediments from Calabrian Selected Areas, Southern Italy. International Journal of Environmental Research, 2019, 13, 571-580.	2.3	6
20	Radiological assessment, mineralogy and geochemistry of the heavy-mineral placers from the Calabrian coast (South Italy). Journal of Instrumentation, 2019, 14, P05015-P05015.	1.2	6
21	Transition Metal Oxides on Reduced Graphene Oxide Nanocomposites: Evaluation of Physicochemical Properties. Journal of Nanomaterials, 2019, 2019, 1-9.	2.7	18
22	Electrospun Nanomaterials for Energy Applications: Recent Advances. Applied Sciences (Switzerland), 2019, 9, 1049.	2.5	49
23	Evaluation of the electrochemical performance of electrospun transition metal oxide-based electrode nanomaterials for water CDI applications. Electrochimica Acta, 2019, 309, 125-139.	5.2	20
24	Role of the carbon defects in the catalytic oxygen reduction by graphite nanoparticles: a spectromagnetic, electrochemical and computational integrated approach. Physical Chemistry Chemical Physics, 2019, 21, 6021-6032.	2.8	27
25	Niobium pentoxide nanomaterials with distorted structures as efficient acid catalysts. Communications Chemistry, 2019, 2, .	4.5	59
26	Shapedâ€controlled siliconâ€doped hematite nanostructures for enhanced PEC water splitting. Catalysis Today, 2019, 328, 43-49.	4.4	24
27	Electrochemical characterization of highly abundant, low cost iron (III) oxide as anode material for sodium-ion rechargeable batteries. Electrochimica Acta, 2018, 269, 367-377.	5.2	26
28	Radioactivity, radiological risk and metal pollution assessment in marine sediments from Calabrian selected areas, southern Italy. European Physical Journal Plus, 2018, 133, 1.	2.6	13
29	Zinc oxide nanocolloids prepared by picosecond pulsed laser ablation in water at different temperatures. EPJ Web of Conferences, 2018, 167, 04008.	0.3	7
30	CO ₂ sensing properties of electro-spun Ca-doped ZnO fibres. Nanotechnology, 2018, 29, 305501.	2.6	24
31	Electro-spun graphene-enriched carbon fibres with high nitrogen-contents for electrochemical water desalination. Desalination, 2018, 428, 40-49.	8.2	34
32	Trimetallic Ni-Based Catalysts over Gadolinia-Doped Ceria for Green Fuel Production. Catalysts, 2018, 8, 435.	3.5	20
33	Synergistic Effects of Active Sites' Nature and Hydrophilicity on the Oxygen Reduction Reaction Activity of Pt-Free Catalysts. Nanomaterials, 2018, 8, 643.	4.1	11
34	Are Electrospun Fibrous Membranes Relevant Electrode Materials for Liâ€Ion Batteries? The Case of the C/Ge/GeO ₂ Composite Fibers. Advanced Functional Materials, 2018, 28, 1800938.	14.9	22
35	Synthesis and characterization of Fe2O3 /reduced graphene oxide nanocomposite as a high-performance anode material for sodium-ion batteries. Modelling, Measurement and Control B: Solid and Fluid Mechanics and Thermics, Mechanical Systems, 2018, 87, 129-134.	0.4	6
36	Effect of calcium- and/or aluminum-incorporation on morphological, structural and photoluminescence properties of electro-spun zinc oxide fibers. Materials Research Bulletin, 2017, 92, 9-18.	5.2	15

#	Article	IF	CITATIONS
37	Effect of Ti- or Si-doping on nanostructure and photo-electro-chemical activity of electro-spun iron oxide fibres. International Journal of Hydrogen Energy, 2017, 42, 28070-28081.	7.1	8
38	Electro-spun Co3O4 anode material for Na-ion rechargeable batteries. Solid State Ionics, 2017, 309, 41-47.	2.7	22
39	Electrospun C/GeO 2 paper-like electrodes forÂflexible Li-ion batteries. International Journal of Hydrogen Energy, 2017, 42, 28102-28112.	7.1	22
40	Controlled surface functionalization of carbon nanotubes by nitric acid vapors generated from sub-azeotropic solution. Surface and Interface Analysis, 2016, 48, 17-25.	1.8	21
41	Origin of the different behavior of some platinum decorated nanocarbons towards the electrochemical oxidation of hydrogen peroxide. Materials Chemistry and Physics, 2016, 184, 269-278.	4.0	14
42	Are Electrospun Carbon/Metal Oxide Composite Fibers Relevant Electrode Materials for Li-Ion Batteries?. Journal of the Electrochemical Society, 2016, 163, A2930-A2937.	2.9	19
43	Enhanced optical response of ZnO/Ag nanocolloids prepared by a picosecond laser. Journal of Luminescence, 2016, 178, 204-209.	3.1	8
44	Characterisation and H 2 O 2 sensing properties of TiO 2 -CNTs/Pt electro-catalysts. Materials Chemistry and Physics, 2016, 170, 129-137.	4.0	22
45	Interplay of structural and magnetic nanoscale phase separation in layered cobaltites. Physical Review B, 2015, 92, .	3.2	5
46	Stabilization of Titanium Dioxide Nanoparticles at the Surface of Carbon Nanomaterials Promoted by Microwave Heating. Chemistry - A European Journal, 2015, 21, 14901-14910.	3.3	12
47	Chemical Modification of Graphene Oxide through Diazonium Chemistry and Its Influence on the Structure–Property Relationships of Graphene Oxide–Iron Oxide Nanocomposites. Chemistry - A European Journal, 2015, 21, 12465-12474.	3.3	38
48	Surface Chemistry and Thermal Stability in Air of Carbon Nanotubes Functionalised via a Novel Eco-Friendly Approach to HNO ₃ Vapor Oxidation. Fullerenes Nanotubes and Carbon Nanostructures, 2015, 23, 83-92.	2.1	2
49	Synthesis of three-dimensional macro-porous networks of carbon nanotubes by chemical vapor deposition of methane on Co/Mo/Mg catalyst. Applied Catalysis A: General, 2015, 505, 487-493.	4.3	10
50	A new approach to the synthesis of titania nano-powders enriched with very high contents of carbon nanotubes by electro-spinning. Materials Chemistry and Physics, 2015, 153, 338-345.	4.0	13
51	Highly Versatile and Efficient Process for CNT Oxidation in Vapor Phase by Means of Mg(NO3)2‒HNO3‒H2O Ternary Mixture. Fullerenes Nanotubes and Carbon Nanostructures, 2015, 23, 1-5.	2.1	7
52	On the Amorphisation Trajectory of Carbon Nanotubes. Materials Research Society Symposia Proceedings, 2014, 1700, 9-14.	0.1	0
53	Fast growth of polycrystalline graphene by chemical vapor deposition of ethanol on copper. , 2014, , .		3
54	A safer and flexible method for the oxygen functionalization of carbon nanotubes by nitric acid vapors. Applied Surface Science, 2014, 303, 446-455.	6.1	17

#	Article	IF	CITATIONS
55	Taguchi optimized synthesis of graphene films by copper catalyzed ethanol decomposition. Diamond and Related Materials, 2014, 41, 73-78.	3.9	29
56	Micro-Raman Analysis of Three-Dimensional Macroporous Sponge-Like Network of Carbon Nanotubes under Tension. Journal of Physical Chemistry C, 2014, 118, 13912-13919.	3.1	2
57	Influence of the Cobalt Phase on the Highly Efficient Growth of MWNTs. Nanomaterials and Nanotechnology, 2014, 4, 5.	3.0	4
58	High-Temperature Growth of Graphene Films on Copper Foils by Ethanol Chemical Vapor Deposition. Journal of Physical Chemistry C, 2013, 117, 21569-21576.	3.1	68
59	Microstructure of anatase-based hybrid nanocomposites. Journal Physics D: Applied Physics, 2013, 46, 125303.	2.8	4
60	Correlation between carbon nanotube microstructure and their catalytic efficiency towards the p-coumaric acid degradation. Current Applied Physics, 2013, 13, 748-752.	2.4	10
61	On the hydrogen sensing mechanism of Pt/TiO2/CNTs based devices. Sensors and Actuators B: Chemical, 2013, 178, 473-484.	7.8	46
62	Evaluation of the Overall Crystalline Quality of Amorphous Carbon Containing Multiwalled Nanotubes. Journal of Physical Chemistry C, 2013, 117, 4815-4823.	3.1	23
63	Do Nanotubes Follow an Amorphization Trajectory as Other Nanocarbons Do?. Journal of Physical Chemistry C, 2013, 117, 14206-14212.	3.1	4
64	Optimized CVD Production of CNT-Based Nanohybrids by Taguchi Robust Design. Journal of Nanoscience and Nanotechnology, 2012, 12, 2424-2436.	0.9	2
65	Growth and Analysis of C Nanotubes on Ceramic Polymer-Additives. Journal of Nanoscience and Nanotechnology, 2012, 12, 4786-4797.	0.9	2
66	Raman scattering in boron-doped single-crystal diamond used to fabricate Schottky diode detectors. Journal of Quantitative Spectroscopy and Radiative Transfer, 2012, 113, 2476-2481.	2.3	17
67	Effect of Fe load on the synthesis of C nanotubes by isobutane decomposition over Na-exchanged montmorillonite-clay catalysts. Diamond and Related Materials, 2012, 23, 54-60.	3.9	4
68	Microâ€Raman and photoluminescence analysis of composite vanadium oxide/polyâ€vinyl acetate fibres synthesised by electroâ€spinning. Journal of Raman Spectroscopy, 2012, 43, 761-768.	2.5	53
69	Effect of sulphuric–nitric acid mixture composition on surface chemistry and structural evolution of liquidâ€phase oxidised carbon nanotubes. Journal of Raman Spectroscopy, 2012, 43, 1432-1442.	2.5	52
70	Effect of Nature and Location of Defects on Bandgap Narrowing in Black TiO ₂ Nanoparticles. Journal of the American Chemical Society, 2012, 134, 7600-7603.	13.7	1,464
71	Hydrogen sensing characteristics of Pt/TiO 2 /MWCNTs composites. International Journal of Hydrogen Energy, 2012, 37, 1842-1851.	7.1	68
72	Influence of reaction parameters on the activity of ruthenium based catalysts for glycerol steam reforming. Applied Catalysis B: Environmental, 2012, 121-122, 40-49.	20.2	63

#	Article	IF	CITATIONS
73	Optimization of CVD growth of CNT-based hybrids using the Taguchi method. Materials Research Bulletin, 2012, 47, 595-601.	5.2	14
74	Synthesis and analysis of multi-walled carbon nanotubes/oxides hybrid materials for polymer composite applications. Diamond and Related Materials, 2011, 20, 532-537.	3.9	5
75	Catalytic Wet Air Oxidation of <i>p</i> -Coumaric Acid over Carbon Nanotubes and Activated Carbon. Industrial & Engineering Chemistry Research, 2011, 50, 9043-9053.	3.7	29
76	Polylactide and carbon nanotubes/smectite-clay nanocomposites: Preparation, characterization, sorptive and electrical properties. Applied Clay Science, 2011, 53, 188-194.	5.2	48
77	On the CVD Growth of C Nanotubes over Fe-Loaded Montmorillonite Catalysts. Nanomaterials and Nanotechnology, 2011, 1, 15.	3.0	4
78	Evaluation of crystalline perfection degree of multiâ€walled carbon nanotubes: correlations between thermal kinetic analysis and microâ€Raman spectroscopy. Journal of Raman Spectroscopy, 2011, 42, 593-602.	2.5	80
79	Room Temperature Hydrogen Sensor Based on Pt/TiO2/MWCNT Composites. Lecture Notes in Electrical Engineering, 2011, , 87-91.	0.4	0
80	Scaling Laws for Multi-Walled Carbon Nanotube Growth by Catalyzed Chemical Vapor Deposition. Journal of Nanoscience and Nanotechnology, 2010, 10, 1286-1295.	0.9	2
81	Calibration of reaction parameters for the improvement of thermal stability and crystalline quality of multi-walled carbon nanotubes. Journal of Materials Science, 2010, 45, 783-792.	3.7	16
82	Crystalline Quality Evaluation of Carbon Nanotubes by Kinetic Analysis in Quasiâ€Isothermal Conditions. ChemPhysChem, 2010, 11, 1925-1931.	2.1	4
83	Feâ€catalysed synthesis of C nanotubes by <i>i</i> â€C ₄ H ₁₀ decomposition: Advantages and problems deriving from H ₂ addition to the growth ambient. Physica Status Solidi (A) Applications and Materials Science, 2010, 207, 1887-1894.	1.8	0
84	Preparation of nanotubes-clay hybrid systems by iron-catalyzed isobutane decomposition. Diamond and Related Materials, 2010, 19, 599-603.	3.9	9
85	K10 Montmorillonite Based Catalysts for the Growth of Multiwalled Carbon Nanotubes through Catalytic Chemical Vapor Deposition. Industrial & Engineering Chemistry Research, 2010, 49, 3242-3249.	3.7	17
86	Micro-Raman analysis of titanium oxide/carbon nanotubes-based nanocomposites for hydrogen sensing applications. Journal of Solid State Chemistry, 2010, 183, 2451-2455.	2.9	44
87	Micro-Raman investigation of vanadium-oxide coated tubular carbon nanofibers for gas-sensing applications. Diamond and Related Materials, 2010, 19, 590-594.	3.9	29
88	Single-crystal diamond MIS diode for deep UV detection. Radiation Effects and Defects in Solids, 2010, 165, 737-745.	1.2	5
89	Enhanced Raman gain coefficients and bandwidths of sodium-niobium-phosphate glasses for Raman gain media. , 2009, , .		2
90	Raman gain in niobium-phosphate glasses. Applied Physics Letters, 2009, 94, .	3.3	36

6

#	Article	IF	CITATIONS
91	Exciton condensation in homoepitaxial chemical vapor deposition diamond. Journal of Applied Physics, 2009, 106, 053528.	2.5	10
92	Influence of gas-mixture composition on yield, purity and morphology of carbon nanotubes grown by catalytic isobutane-decomposition. Diamond and Related Materials, 2009, 18, 360-363.	3.9	6
93	Influence of Carbon Source and Fe-Catalyst Support on the Growth of Multi-Walled Carbon Nanotubes. Journal of Nanoscience and Nanotechnology, 2009, 9, 3815-3823.	0.9	31
94	Multiâ€walled carbon nanotubes production by ethane decomposition over silicaâ€supported ironâ€catalysts. Physica Status Solidi (A) Applications and Materials Science, 2008, 205, 2422-2427.	1.8	8
95	Raman analysis of MWCNTs produced by catalytic CVD: derivation of a scaling law for the growth parameters. Journal of Raman Spectroscopy, 2008, 39, 141-146.	2.5	4
96	Study of strain and wetting phenomena in porous silicon by Raman scattering. Journal of Raman Spectroscopy, 2008, 39, 199-204.	2.5	32
97	Raman and photoluminescence study of hot filament CVD diamond films grown on WC–Co substrates. Journal of Raman Spectroscopy, 2008, 39, 157-163.	2.5	6
98	Experiments on C nanotubes synthesis by Fe-assisted ethane decomposition. Diamond and Related Materials, 2008, 17, 318-324.	3.9	17
99	Large-scale production of high-quality multi-walled carbon nanotubes: Role of precursor gas and of Fe-catalyst support. Diamond and Related Materials, 2008, 17, 1482-1488.	3.9	45
100	Spectroscopic investigation of homoepitaxial CVD diamond for detection applications. Diamond and Related Materials, 2008, 17, 372-376.	3.9	2
101	Investigation of Porous Silicon Wetting by Raman Scattering. Spectroscopy Letters, 2008, 41, 174-178.	1.0	2
102	On the correlation between CVD growth conditions and crystalline quality and abundance of multi-walled carbon nanotubes. EPJ Applied Physics, 2008, 41, 237-242.	0.7	5
103	Iron-catalyst performances in carbon nanotube growth by chemical vapour deposition. EPJ Applied Physics, 2008, 44, 171-180.	0.7	4
104	Aid of Raman spectroscopy in diagnostics of MWCNT synthesised by Fe-catalysed CVD. Journal of Physics: Conference Series, 2007, 61, 931-935.	0.4	14
105	Measurements of adsorption strain in porous silicon by Raman scattering. , 2007, , .		2
106	Study of the effects on the Raman spectra of adsorption strain in porous silicon. , 2007, , .		0
107	Optimisation of gas mixture composition for the preparation of high quality MWCNT by catalytically assisted CVD. Diamond and Related Materials, 2007, 16, 1095-1100.	3.9	34
108	Yield And Quality Optimization For MWNT Prepared By Catalytic CVD. AIP Conference Proceedings, 2007, , .	0.4	0

#	Article	IF	CITATIONS
109	Single crystal diamond detectors grown by chemical vapor deposition. Nuclear Instruments and Methods in Physics Research, Section A: Accelerators, Spectrometers, Detectors and Associated Equipment, 2007, 570, 299-302.	1.6	12
110	Analysis of trapping–detrapping defects in high quality single crystal diamond films grown by Chemical Vapor Deposition. Diamond and Related Materials, 2006, 15, 1878-1881.	3.9	3
111	Characterization of homoepitaxial CVD diamond grown at moderate microwave power. Diamond and Related Materials, 2006, 15, 517-521.	3.9	3
112	Pulse height defect in pCVD and scCVD diamond based detectors. Diamond and Related Materials, 2006, 15, 1986-1989.	3.9	4
113	Homoepitaxial CVD diamond: Raman and time-resolved PL characterization. Diamond and Related Materials, 2006, 15, 1976-1979.	3.9	10
114	Characterization of homoepitaxial diamond for ionizing radiation detectors. Journal of Non-Crystalline Solids, 2006, 352, 2575-2579.	3.1	3
115	Study of in-gap defects in intrinsic and B-doped a-Si1â^'xCx:H by photo-induced optical absorption and photoluminescence. Journal of Non-Crystalline Solids, 2006, 352, 2647-2651.	3.1	1
116	Optical Characterisation of High-Quality Homoepitaxial Diamond. Topics in Applied Physics, 2006, , 345-358.	0.8	2
117	Diamond-based photoconductors for deep UV detection. Nuclear Instruments and Methods in Physics Research, Section A: Accelerators, Spectrometers, Detectors and Associated Equipment, 2006, 567, 188-191.	1.6	12
118	Multi-wavelength Raman investigation of sputtered a-C film nanostructure. Surface and Coatings Technology, 2006, 200, 5427-5434.	4.8	6
119	Low-frequency Raman study of hollow multiwalled nanotubes grown by Fe-catalyzed chemical vapor deposition. Journal of Applied Physics, 2006, 100, 104311.	2.5	24
120	Semi-empirical derivation of the physical approximants to a-CN:H film deposition. Diamond and Related Materials, 2005, 14, 1331-1341.	3.9	1
121	A single growth quality indicator for film property tailoring. Diamond and Related Materials, 2004, 13, 1391-1397.	3.9	2
122	Raman and photoluminescence analysis of CVD diamond films: influence of Si-related luminescence centre on the film detection properties. Diamond and Related Materials, 2004, 13, 923-928.	3.9	18
123	Photoconductive properties of single-crystal CVD diamond. Physica Status Solidi A, 2003, 199, 113-118.	1.7	12
124	A qualitative indicator for preliminary diagnostics of a-C based coatings. Physica Status Solidi A, 2003, 199, 335-346.	1.7	1
125	Spectral response of large area CVD diamond photoconductors for space applications in the vacuum UV. Diamond and Related Materials, 2003, 12, 1819-1824.	3.9	9
126	A single quality factor for the deposition process of reactively sputtered thin a-C:H:N films. Journal of Non-Crystalline Solids, 2003, 318, 322-330.	3.1	2

#	Article	IF	CITATIONS
127	Vibrational properties and microstructure of reactively sputtered hydrogenated carbon nitrides. Journal of Applied Physics, 2002, 91, 1155-1165.	2.5	70
128	Effects of hydrogen incorporation on structural relaxation and vibrational properties of a-CN:H thin films grown by reactive sputtering. Diamond and Related Materials, 2002, 11, 1166-1171.	3.9	7
129	Relationship between composition and position of Raman and IR peaks in amorphous carbon alloys. Surface and Coatings Technology, 2002, 151-152, 257-262.	4.8	31
130	Evidence for the existence of scaling laws correlating the deposition parameters and the Raman spectra features in thin a-C:N:H films deposited by reactive r.f. sputtering. Vacuum, 2002, 67, 537-542.	3.5	3
131	Influence of metal–diamond interfaces on the response of UV photoconductors. Diamond and Related Materials, 2001, 10, 698-705.	3.9	15
132	A joint macro-/micro- Raman investigation of the diamond lineshape in CVD films: the influence of texturing and stress. Diamond and Related Materials, 2001, 10, 1535-1543.	3.9	13
133	High quality CVD diamond for detection applications: structural characterization. Diamond and Related Materials, 2001, 10, 1788-1793.	3.9	17
134	High quality CVD diamond: a Raman scattering and photoluminescence study. European Physical Journal B, 2001, 20, 133-139.	1.5	31
135	Nature of non-D and non-G bands in Raman spectra of a-C:H(N) films grown by reactive sputtering. Journal of Applied Physics, 2001, 89, 1053-1058.	2.5	30
136	Structural and Functional Characterization of HPHT Diamond Crystals Used in Photoconductive Devices. Physica Status Solidi A, 2000, 181, 91-97.	1.7	4
137	Role of the film texturing on the response of particle detectors based on CVD diamond. Microsystem Technologies, 1999, 5, 151-156.	2.0	7
138	Structural characterisation of ionising-radiation detectors based on CVD diamond films. Microsystem Technologies, 1999, 6, 23-29.	2.0	15
139	Raman characterisation and hardness properties of diamond-like carbon films grown by pulsed laser deposition technique. Microsystem Technologies, 1999, 6, 30-36.	2.0	3
140	Comparative study of band-A cathodoluminescence and Raman spectroscopy in CVD diamond films. Diamond and Related Materials, 1999, 8, 640-644.	3.9	8
141	Nature of band-A cathodoluminescence inCVD diamond films. Nuovo Cimento Della Societa Italiana Di Fisica D - Condensed Matter, Atomic, Molecular and Chemical Physics, Biophysics, 1998, 20, 1193-1200.	0.4	1
142	Numerical approximation of the physical laws governing scattering in electron beam lithography. Nuovo Cimento Della Societa Italiana Di Fisica D - Condensed Matter, Atomic, Molecular and Chemical Physics, Biophysics, 1998, 20, 1201-1208.	0.4	2
143	Physical approximants to electron scattering. Microelectronic Engineering, 1997, 34, 147-154.	2.4	11
144	Application of the Î theorem of dimensional analysis to electron scattering in multi-component systems. Nuovo Cimento Della Societa Italiana Di Fisica D - Condensed Matter, Atomic, Molecular and Chemical Physics, Biophysics, 1996, 18, 1005-1018.	0.4	2

#	Article	IF	CITATIONS
145	«Buckingham» approximants to physical laws. Nuovo Cimento Della Societa Italiana Di Fisica D - Condensed Matter, Atomic, Molecular and Chemical Physics, Biophysics, 1995, 17, 523-535.	0.4	1
146	A single quality factor for electron backscattering from thin films. Microelectronic Engineering, 1995, 27, 183-186.	2.4	1
147	Monte Carlo modelling of electron beam lithography: a scaling law. Microsystem Technologies, 1994, 1, 23-29.	2.0	8
148	The role of electron scattering in x-ray reflection masks. Microelectronic Engineering, 1994, 26, 49-61.	2.4	0
149	Tungsten/carbon masks in x-ray projection lithography. Microelectronic Engineering, 1994, 23, 421-425.	2.4	0
150	Simulation of electron-scattering properties of diamond membranes in X-ray mask fabrication. Diamond and Related Materials, 1994, 3, 942-946.	3.9	0
151	Short-range and long-range scattering in electron beam lithography. Microelectronic Engineering, 1993, 20, 241-253.	2.4	5
152	Electron scattering of low-Z high-density materials in X-ray mask patterning. Microelectronic Engineering, 1993, 20, 291-304.	2.4	0
153	Electron scattering of diamond membranes in x-ray mask fabrication. Microelectronic Engineering, 1993, 21, 91-94.	2.4	Ο
154	Perspectives in electron scattering by microstructures. Nuovo Cimento Della Societa Italiana Di Fisica D - Condensed Matter, Atomic, Molecular and Chemical Physics, Biophysics, 1993, 15, 531-539.	0.4	0
155	Experimental test of high-resolution process modelling in electron beam lithography at 25 to 50 keV. Nuovo Cimento Della Societa Italiana Di Fisica D - Condensed Matter, Atomic, Molecular and Chemical Physics, Biophysics, 1993, 15, 1345-1359.	0.4	1
156	The generalized backscattering coefficient: A novel parameter in electron scattering processes. Microelectronic Engineering, 1992, 17, 385-388.	2.4	6
157	Electron scattering in microstructure processes. Rivista Del Nuovo Cimento, 1992, 15, 1-57.	5.7	17
158	Electron scattering effects in additive patterning of XRL masks for 0.2 micron resolution. Microelectronic Engineering, 1991, 13, 197-200.	2.4	2
159	Monte Carlo analysis of electron scattering in microstructure processes in the 0.2 μm region. Nuovo Cimento Della Societa Italiana Di Fisica D - Condensed Matter, Atomic, Molecular and Chemical Physics, Biophysics, 1991, 13, 1049-1059.	0.4	2
160	Modeling of electron beam scattering in high resolution lithography for the fabrication of X-Ray masks. European Transactions on Telecommunications, 1990, 1, 143-147.	1.2	0
161	Simulation of 64 megabit lithography in XRL masks obtained by single-layer process on Si substrates. Microelectronic Engineering, 1990, 11, 625-628.	2.4	7
162	X-ray mask making by EBL and Monte Carlo analysis of a single-resist layer process on low-z membrane. Microelectronic Engineering, 1989, 9, 147-150.	2.4	7

#	Article	IF	CITATIONS
163	Electronic conduction in the layered semiconductor MnPS3. Journal of Physics Condensed Matter, 1989, 1, 3337-3347.	1.8	25
164	Electronic transport properties of NiPS3. Physical Review B, 1988, 37, 4419-4424.	3.2	23
165	Optical absorption spectra of some transition metal thiophosphates. Solid State Ionics, 1986, 20, 9-15.	2.7	37
166	M2, 3 absorption spectra of transition metal ion in MnPS3, FePS3 and NiPS3. Solid State Communications, 1986, 60, 381-384.	1.9	11
167	Valence and conduction bands in MPS3 layered compounds studied by synchrotron radiation. Nuovo Cimento Della Societa Italiana Di Fisica D - Condensed Matter, Atomic, Molecular and Chemical Physics, Biophysics, 1986, 8, 263-278.	0.4	5
168	Soft x-ray absorption of FePS3 and NiPS3. Solid State Communications, 1984, 51, 467-472.	1.9	29
169	Study of the valence bands of FePS3 and NiPS3 by resonant-photoemission spectroscopy. Nuovo Cimento Della Societa Italiana Di Fisica D - Condensed Matter, Atomic, Molecular and Chemical Physics, Biophysics, 1984, 4, 444-452.	0.4	16
170	Nucleation Process of CVD Diamond on Molybdenum Substrates. , 0, , 329-343.		1
171	Aid of Scaling Laws in the Achievement of a Well-Controlled Film Deposition Process. , 0, , 1-21.		63